



Design of achromatic surface microstructure for near-eye display with diffractive waveguide[☆]

Jiasheng Xiao^a, Juan Liu^{a,*}, Jian Han^b, Yongtian Wang^a

^a Beijing Engineering Research Center for Mixed Reality and Advanced Display, School of Optics and Photonic, Beijing Institute of Technology, Beijing, 100081, China

^b Key Laboratory of Information System and Technology, Beijing Institute of Control and Electronic Technology, Beijing, 100038, China

ARTICLE INFO

Keywords:

Holographic optical elements
Heads-up displays
Augmented reality

ABSTRACT

Dispersion problem has always constrained the development of see-through near-eye displays with diffractive waveguide. Here, we propose a design method and optical systems for one-layer achromatic surface microstructure composed with a triple-carved-sub-grating. The triple-carved-sub-grating with specified period is designed based on rigorous coupled wave theory, corresponding to Red (R), Green (G) and Blue (B) wavelengths, respectively. The surface microstructure with period of 18.9μm is realized by synthesizing the three sub-gratings together, and it is verified numerically that the diffractive angle of R, G, and B wavelengths is 35° under the normal incidence of TE polarization, which imply that the surface microstructure diffracts the certain RGB wavelengths achromatically. A diffraction waveguide with achromatic surface microstructure is also modeled to analysis the stray light and color correction, and the results indicate that the diffraction waveguide transmits image with little stray light. Via proper duplication it could be utilized as the combining optics of diffractive-waveguide near-eye display and head-up display because of its light and compact features.

1. Introduction

See-through near-eye display (NED) is becoming a hot topic because of its various applications in both commercial and defense market [1,2]. By series of technical ways, researchers intend to make the NED as small and lightweight as the ordinary sunglasses [3–6]. Among all those technologies, using a transparent diffractive waveguide or diffractive optical element (DOE) as the optical combiner can dramatically reduce the weight and size of NED [7–10]. However, there still exist some problems which need to be solved, in aspect of imaging, the most important one is dispersion problem resulting from DOE when the NED displays a full-color image.

Some potential diffractive optical components could be applied to NEDs for chromatic elimination. Metasurface is one innovative flat optical component constructed with subwavelength structures, which provides a new means to manipulate the amplitude, phase, polarization of light, etc. Aieta et al. [11] and Mohammadreza et al. [12] proposed the multi-wavelength achromatic metasurfaces with dielectric material, which is thin, lightweight and suitable for wearable glasses, whereas the achromatic metasurfaces can only be used for infrared waveband. Deng et al. [13] used a single-layer metasurface to realize achromatic diffraction, but the cost of metasurface as well as the low transmittance of visible light limit its application in NEDs. Specifically,

focusing on the dispersion problem in diffractive near-eye display, some researchers have offered some feasible proposals. In holographic ways, Sony Corporation [14] proposed an achromatic design with three stacks of holographic films responding to red, green, and blue wavelengths, respectively. Shi et al. [15] developed three-step exposure and Zhang et al. [16] developed volume hologram–plane hologram combination to achieve achromatic display, but the inherent color shift of hologram seriously restricts the experimental performance. BAE System [17] disclosed their achromatic waveguide patent recently, which shows they adopted two electronically switchable Bragg gratings (ESBGs) [18] served as red hologram and blue hologram, respectively, to compensate dispersion, whereas ESBGs need high driving voltage. In lithographic ways, Microsoft's HoloLens [19] employed a three-stack optical waveguide, each of that diffracts RGB waveband, respectively. With final color matching, a full-color image can be generated, however, this scheme makes the optical system bulky and heavier.

Here we propose a design method to eliminate the dispersion and optical waveguide system with achromatic surface microstructure based on rigorous coupled wave theory and grating multiplexing, which diffracts RGB lights achromatically at desired angle. The surface microstructure could be served as the input/output couplers in diffractive near-eye displays to solve the problem of full-color display with only

[☆] Jiasheng Xiao and Jian Han have made equal contributions to this research work.

* Corresponding author.

E-mail address: juanliu@bit.edu.cn (J. Liu).

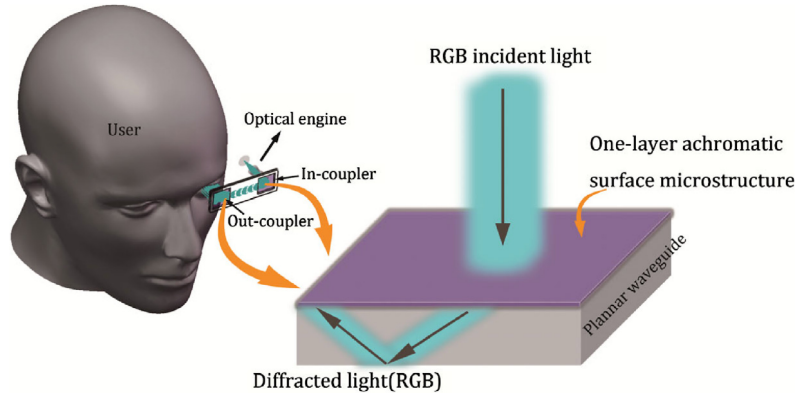


Fig. 1. Scheme of diffractive near-eye display with achromatic surface microstructure. Achromatic surface microstructure serves as the in-coupler and out-coupler, and it diffracts RGB wavelengths to the same diffractive angle.

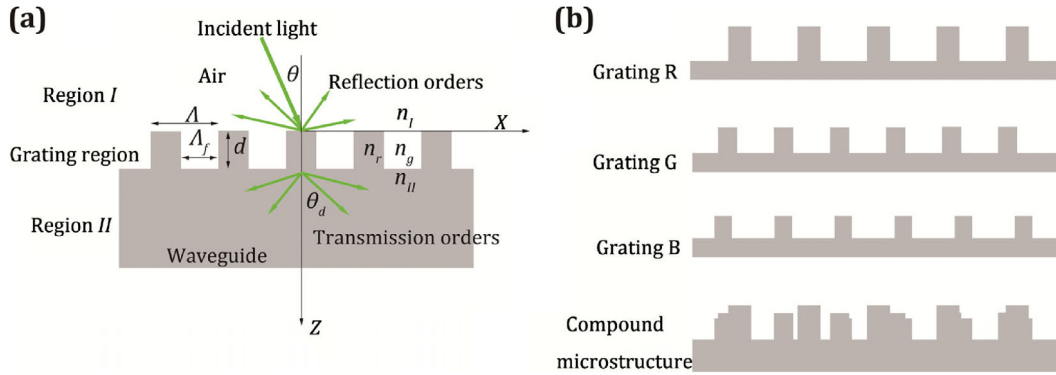


Fig. 2. (a) Schematic of rectangular sub-grating. Incident light from the air (region I) with incident angle θ is diffracted by the grating (grating region) into the waveguide substrate (region II). (b) Illustration of the sub-gratings and compound microstructure. Grating R, Grating G and Grating B represent sub-gratings for RGB wavelengths, respectively. The compound microstructure is composed with the triple-carved-sub-grating by synthesizing them.

one stack of planar optical waveguide, which can dramatically reduce the weight and size of NEDs.

2. Materials and methods

2.1. General scheme

A sketch of the achromatic waveguide display system is shown in Fig. 1. The RGB lights emitted from the optical engine and coupled into the waveguide by the in-coupler, and then propagate along the waveguide in the condition of total internal reflection (TIR). When the lights hit the out-coupler, they are diffracted out of the waveguide and finally enter the human eye. The key part of this system is the achromatic in-coupler and out-coupler of waveguide, and we describe the basic design of the waveguide as follows.

The waveguide contains two one-layer microstructures carved on the top surface, and each of them is a triple overlapping etching grating, coupling light in or out of the waveguide without chromatic aberration, as shown in Fig. 1. The design of the microstructure should be constrained by the following terms. (1) The diffraction angle should be greater than the TIR critical angle of the waveguide. (2) The structure of in or out coupler is same. (3) The couplers and waveguide use same material. (4) Three discrete wavelengths representing red, green, and blue light, respectively, are diffracted by the microstructure with the same angle. These constraints guarantee the achromatic microstructure can be applied to waveguide display and easily fabricated. Here, we choose rectangular grating as the basic component of the microstructure due to it can be designed to diffract light by a desired angle for one particular wavelength. If we use three sub-gratings to diffract three different wavelengths in same angle as well as satisfy the TIR angle of

the waveguide, achromatic coupling will be realized. With appropriate design to overlap these gratings together, the coupler of the waveguide can be developed.

2.2. Design theory

Traditional holographic wavelength multiplexing is based on the cosine phase grating. Here, rectangular gratings are chosen as the basic component for our design, which is easy to process for micro-nano technology, and they can be designed based on rigorous coupled wave theory(RCWA) [20]. The transmission rectangular sub-gratings for RGB wavelengths are described in Fig. 2(a), with period Λ , depth d , the refractive index of ridge n_r and groove n_g , and duty cycle f . The incident light propagates in XZ plane with wavelength λ , the index of incident region is n_g and the index of diffraction region is n_r . And the grating equation is written as:

$$n_g \sin \theta - n_r \sin \theta_d = \frac{m_i \lambda_i}{\Lambda_i} \quad \text{for } i = R, G, \text{ and } B \quad (1)$$

where θ and θ_d refer to the incident and diffractive angle, respectively, m_i is the diffraction order, and Λ_i , λ_i , n_g , and n_r define the period, wavelength, the index of incident and diffraction region as described above.

The core of achromatism is to keep the value on the left equation unchanged at different wavelengths λ_i . If the triple-carved-sub-grating with three specified periods, corresponding to RGB wavelengths, owns the least common period, which is an integral multiple (N_i) of three specified periods respectively, the diffraction light of the sub-gratings will be modulated at desired directions in the triple-carved-sub-grating when the order m_i times an corresponding integer N_i . According to the

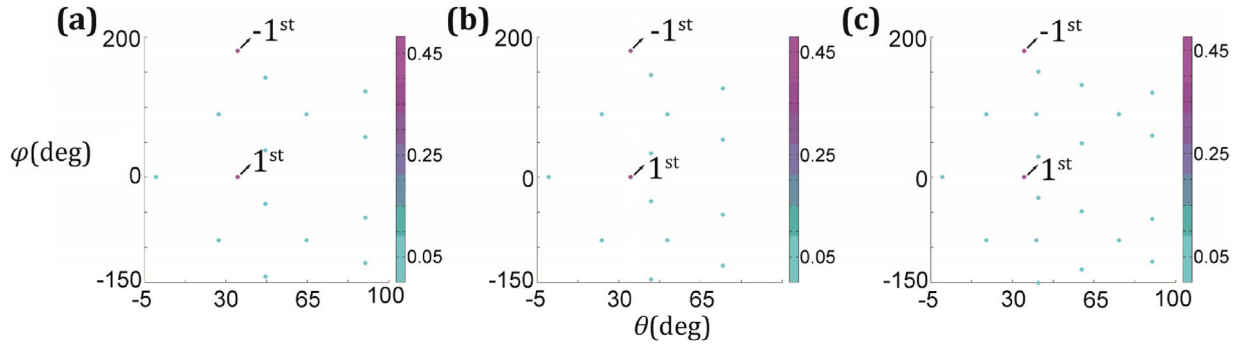


Fig. 3. Distribution of diffraction orders. (a), (b), and (c) are the scatterplots of diffraction orders for RGB sub-gratings under TE polarization, respectively. θ and φ refer to the polar angle and azimuthal angle in spherical coordinate system.

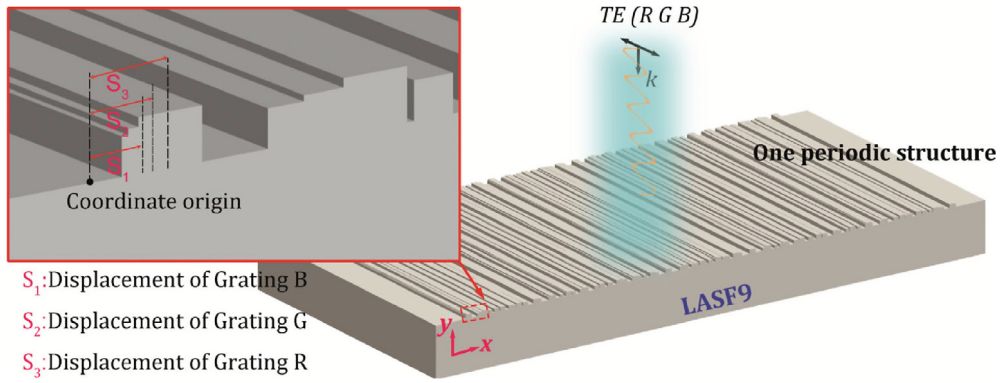


Fig. 4. Simulation model of the surface microstructure. One period structure is calculated under the periodic boundary condition, with TE polarization incidence. S_1 , S_2 and S_3 refer to the displacement of RGB sub-gratings from the global coordinate origin, respectively.

design demand, the wavelength λ_i will be calculated after θ , θ_d , Λ_i , n_g , n_r are decided, then the parameters of the sub-gratings need to be optimized until we find the maximum diffraction efficiency to maximize the performance of the sub-gratings. The diffraction efficiencies of the i th order reflected wave and transmitted wave under TE polarization and TM polarization are defined as:

$$\eta_{TERi} = R_i R_i^* \text{Re} \left(\frac{k_{I,zi}}{n_I k_0 \cos \theta} \right) \quad (2)$$

$$\eta_{TMRi} = R_i R_i^* \text{Re} \left(\frac{k_{I,zi}}{n_I k_0 \cos \theta} \right) \quad (3)$$

$$\eta_{TEti} = T_i T_i^* \text{Re} \left(\frac{k_{II,zi}}{n_I k_0 \cos \theta} \right) \quad (4)$$

$$\eta_{TMti} = T_i T_i^* \text{Re} \left(\frac{n_I k_{II,zi}}{n_I^2 k_0 \cos \theta} \right) \quad (5)$$

here R_i is the normalized electric-field amplitude of the i th reflected wave, and T_i is the normalized electric-field amplitude of the transmitted wave. Both of them are in relationship with period Λ , depth d and duty cycle f . $k_{I,zi}$ and $k_{II,zi}$ are reflected and transmitted wave vectors along Z direction, respectively, which are defined as:

$$k_{l,zi} = \begin{cases} \sqrt{(k_0 n_l)^2 - k_{xi}^2} & k_{xi}^2 < (k_0 n_l)^2 \\ -j \sqrt{k_{xi}^2 - (k_0 n_l)^2} & k_{xi}^2 > (k_0 n_l)^2 \end{cases}, \quad l = I, II \quad (6)$$

where $k_{xi} = k_0 [n_I \sin \theta - i(\lambda_0/\Lambda)]$. From Eqs. (2)–(6), we can design high efficiency gratings under TE or TM incidence by finding appropriate grating parameters.

The microstructure for NEDs requires high transmittance and high refractive index of the material in visible wavelength range. According to the principle of NED optics, the collimated RGB lights normally incidence from the air bounces, propagates along the waveguide under

TIR condition after diffracted by surface microstructure (in-coupler). It is a good design start that we first set the diffraction angle which is larger than the critical TIR angle θ_d of the waveguide material. Then the manufacturing capability must be considered beforehand, and we set the periods of RGB gratings to be Λ_r , Λ_g , Λ_b , respectively, which makes their minimum common period to be Λ_c . This setting has following benefits in design and manufacturing stages. First, in the design and analysis stages, only one minimum common period needs to be considered, which is very convenient and time-saving. Second, in the manufacturing and application stages, a mass grating could be applied to NEDs to couple light in and out of waveguide by duplicating.

$$m_i \leq \frac{n_r \Lambda_i}{\lambda_i} \quad \text{for } i = R, G, \text{ and } B \quad (7)$$

After determining the material, the diffraction angle and the grating period, we can design the sub-gratings. To ease the fabrication, we set the grating period approaching to the wavelength, so there exist only three orders (0th, ± 1 st) according to Eq. (7) derived from grating equation. In order to reduce the energy loss, only the first diffraction orders are expected to be existed, which is regarded as the working order, and then the central wavelength of the RGB bands will be derived from the grating equation. According to the spectral characteristics of the rectangular sub-grating, the incident light passes through the sub-grating will produce the symmetry order of the diffraction light with equal energy. So eliminating 0th and other transmission light orders (i.e. higher harmonics) and maximizing the intensity of first-order diffraction light are the issues need to be dealt with. The final surface microstructure composed with Grating R, Grating G and Grating B is realized by integrating them together, i.e. OR (or logic operator) mathematically (see Fig. 2(b)). If the grating period is less than the wavelength, there would be only one order, which will improve the efficiency greatly while it would be a challenge for fabrication.

Table 1

Parameters of the triple-carved-sub-grating under TE polarization.

	Grating R	Grating G	Grating B
Wavelength (μm)	0.666	0.574	0.483
Index	1.8417	1.8522	1.8699
Period (μm)	0.63	0.54	0.45
Ridge height (μm)	0.3007	0.2497	0.2168
Duty cycle	0.3111	0.3126	0.2676
Common period (μm)	18.9		
1st efficiency	0.4820	0.4793	0.4753
0th efficiency	0.0007	0.0056	0.0093
–1st efficiency	0.4820	0.4793	0.4753

2.3. Data analysis

According to the theoretical equations and design flow above, we use MATLAB to build an optimization model and find the best solution by varying the ridge height d and duty cycle f of rectangular sub-gratings for achieving the final grating with maximization the performance of the sub-gratings (i.e. the maximum first-order diffraction efficiency in Eq. (4)). Considering the diffraction modulation, material transparency and manufacturing capacity, LASF9 glass is chosen as the waveguide and grating material in the design. The diffraction angle θ_d is set to be 35° , and the parameters Λ_r , Λ_g , Λ_b are set to be $0.63 \mu\text{m}$, $0.54 \mu\text{m}$ and $0.45 \mu\text{m}$, respectively. The period of the triple-carved-sub-grating Λ_c is the least common multiple (LCM) of the three periods above, which is $18.9 \mu\text{m}$ (see Table 1). Therefore, the corresponding integers are 30, 35, and 42, respectively. As showed in Fig. 3, under the normal incidence of TE polarization, we find that all the sub-gratings diffract lights with almost equal efficiency concentrating upon ± 1 st orders by the same angle, and the 0th and other diffraction orders are successfully suppressed. The grating parameters for the TE polarization are listed in Table 1. The ± 1 st orders diffraction efficiency of sub-gratings for RGB wavelengths are higher than 47.5%, and the 0th order is basically zero. The three discrete wavelengths could refer to RGB lights, respectively. These results shows that the designed sub-gratings meet the previous requirements.

3. Results and discussion

In order to solve the dispersion problem in NEDs, we designed three sub-gratings based on rigorous coupled wave theory. After all the three sub-gratings are calculated separately, surface microstructure can be obtained by superimposing them together (see Fig. 2(b)). We expected to see the achromatic effect of this surface microstructure according to the principle of achromatism, and simulations are performed to verify if this design meets the requirement.

Finite-difference time-domain simulations were performed to analyze its diffraction characters via Lumerical FDTD solutions, as shown in Fig. 4. One remarkable problem is that different displacement of sub-gratings from origin will generate different microstructures in one period, as shown in the zoomed-in view (see Fig. 4). The simulation results show that the surface microstructure is insensitive to the relative displacement of sub-gratings, and Fig. 4 shows one period of the microstructure in which S_1 , S_2 and S_3 are equal half of RGB sub-grating periods, respectively. Fig. 5(a), (b), and (c) show the diffraction angle/diffraction efficiency of final grating for R, G, and B wavelengths before and after optimization, respectively, with diffraction angle between 31° and 39° . It can be seen that RGB light own same diffraction angle at 35° before optimization, which shows that the microstructure achieves achromatism at desired degrees obviously. However, the diffraction efficiencies of RGB wavelengths are not high and some undesired orders are produced, and the main reason for this is that the superimposing of the sub-grating structure is not completely equivalent to the superposition of the sub-grating diffraction function. The Particle Swarm Optimization (PSO) was further adopted to obtain

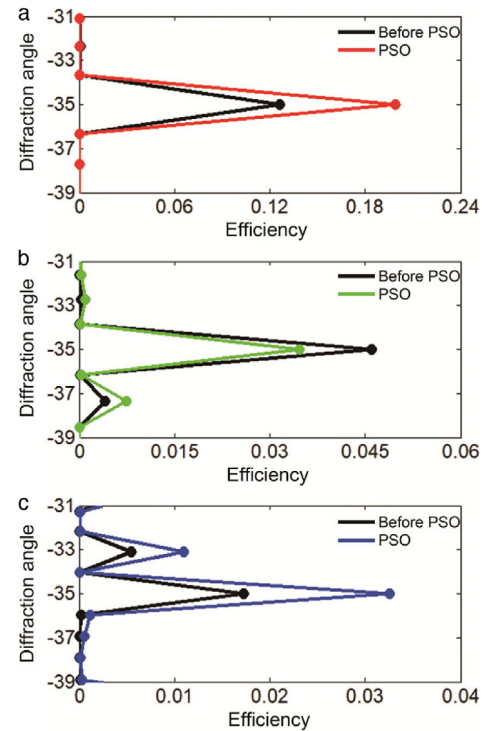


Fig. 5. (a), (b), and (c) show the relationship of diffraction angle and diffraction efficiency for RGB wavelengths between 31° and 39° before and after PSO, respectively.

Table 2

Parameters of the final grating after PSO.

	Grating R	Grating G	Grating B
Ridge height (μm)	0.4000	0.3500	0.3200
Duty cycle	0.3156	0.2000	0.2000

higher diffraction efficiency at desired angle, where the duty cycle and ridge height of RGB sub-gratings serve as independent variables. The diffraction efficiencies after PSO are also shown in Fig. 5. Compared with the results without PSO, the diffraction efficiencies of R and B wavelengths are improved, but the efficiency of green light is slightly lowered. The parameter of the final grating after PSO are listed in Table 2.

The microstructure leads to some weak unwanted orders due to the non-linear sub-gratings superimposing as shown in Fig. 5(b) and (c), which will lead cross-talks for near-eye display system, thus we have to design the diffraction waveguide carefully to reduce the stray light, which will be discussed in Section 4. Fig. 5 also indicate that the diffraction efficiency of RGB light are non-uniform, with the ratio of RGB lights about 7.3:2.7:1 before PSO. Most of the diffraction light focus on the zeroth order and hit the bottom surface of waveguide normally.

4. Ray analysis

The diffraction planar waveguide with achromatic surface microstructure (AcSM) is shown in Fig. 6(a), with AcSM width w , and the thickness of waveguide d . The structure is similar to other diffraction waveguide, such as holographic waveguide [14,15] and surface relief grating waveguide. The AcSM serves as the in-coupler, which deflects the incident light into the waveguide with diffraction angle θ_d . The color lines and gray shaded area refer to the unwanted lower-order light and transmission light in the waveguide, respectively. To reduce the stray light in the waveguide, we adopt two methods. (1) Coating black film. (2) Optimizing the interval of in coupler and

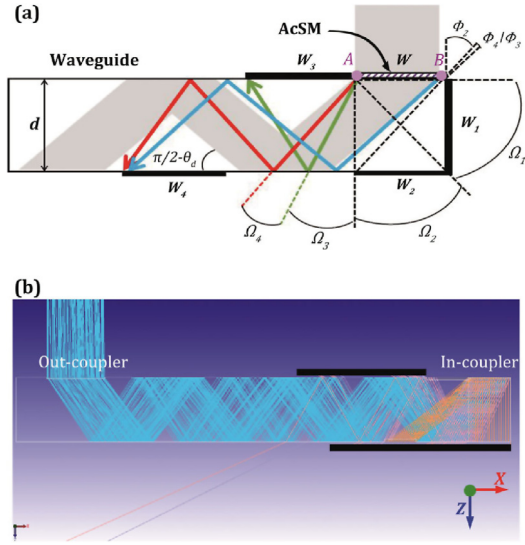


Fig. 6. (a) Sketch of achromatic diffraction planar waveguide with stray light. (b) The model of non-sequence raytrace with black film. (For interpretation of the references to color in this figure legend, the reader is referred to the web version of this article.)

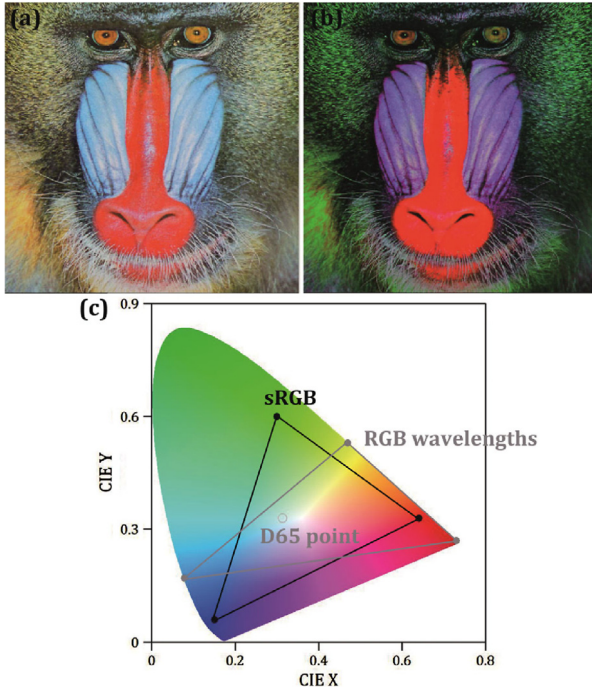


Fig. 7. Color transformation between sRGB color space and RGB wavelengths space. (a) Original image. (b) The transformed image. (c) The color gamut of sRGB and RGB wavelengths color space. (For interpretation of the references to color in this figure legend, the reader is referred to the web version of this article.)

out coupler. Four small areas near AcSM are coated absorber, with width w_1 , w_2 , w_3 and w_4 , respectively, which is necessary and used to absorb unwanted lower-order stray light. The absorber could be the black coating, such as Metal Velvet and Spectral Black, with absorbance 99.99%. The range of stray light corresponding to each absorbing film are showed in Fig. 6(a), specifically, for the left endpoint A of the AcSM, the range Ω_4 , Ω_3 , Ω_2 , Ω_1 correspond to the absorbing areas w_4 , w_3 , w_2 and w_1 , respectively, and for the right endpoint B, the range Φ_2 , Φ_3/Φ_4 correspond to the absorbing areas w_2 , w_3 or w_4 , respectively. To ensure that the transmission light is not absorbed and stray light is absorbed as much as possible, the parameters needs to satisfy the

following constraints:

$$\begin{aligned} w_1 &= d \\ w_2 &= d \tan \theta_1 (w_2 \geq w) \\ w_3 &= 2d \tan \theta_1 - w \\ w_4 &= 3d \tan \theta_1 - w - d \tan \theta_2 \end{aligned} \quad (8)$$

where θ_1 and θ_2 are the limits of diffraction angle θ_d ($\theta_1 < \theta_d < \theta_2$). Additional absorbers could be set to further reduce stray light. Here, we set θ_1 to 33° , which is greater than the total reflection angle 32.3° , and θ_2 to 39° . The thickness of waveguide is set to be 5 mm, and then we can calculate the size of absorber via Eq. (8), $w_1 = 5$ mm, $w_2 = 3.25$ mm, $w_3 = 3.25$ mm and $w_4 = 2.45$ mm. Higher-order stray light can be reduced by optimizing the interval of in coupler and out coupler. Based on the parameters above and results of AcSM, we build a diffraction waveguide model to run optimization and raytrace in OPTIS Optisworks. As shown in Fig. 6(b), the blue lines refer to the light with diffraction angle ranging from 33° to 39° , and the other lines refer to the stray light. The results of non-sequence raytrace show that most of stray light are absorbed or escape from the out-coupler, with the distance of the in coupler and out coupler about 35.4 mm. In addition, stray light escaping from the waveguide can be reduced by an external optomechanical structure, as shown in Fig. 6(b). Color transformation, which is based on CIE 1931xyY color space and the colorimetric standard observer model, is also analyzed to ensure that color images are displayed vividly and correctly. Fig. 7(a) is the original image in sRGB color space, whose RGB components are adjusted according to the diffraction efficiency ratio 7.3:2.7: 1, and Fig. 7(b) is the transformed image of Fig. 7(a) in RGB wavelengths space, where the CIExyz color space is used as the transit space for the conversion [21] and the transformation matrix A from the CIExyz color space to the RGB wavelengths space is as follow, based on the transformation matrix, we can convert the figure of Fig. 7(a) in CIExyz color space to Fig. 7(b).

$$A = \begin{bmatrix} 6.1399 & -5.4986 & 0.6088 \\ -0.8250 & 2.2452 & 0.4234 \\ 0.0010 & -0.0027 & 0.9201 \end{bmatrix}$$

Both Fig. 7(a) and (b) are displayed in sRGB color space. The results show that the components of green yellow in original image are transformed into the second component in RGB wavelengths space successfully and effectively. The color gamut of sRGB and RGB wavelengths are also shown in Fig. 7(c). Comparing to the sRGB, the gamut of RGB wavelengths color space is rotated around D65 point and can display more spectral color.

Comparing with the previous methods [13,14] focusing on full-color near-eye displays, the surface microstructure proposed is one stack composed with one triple-carved-sub-grating, and its periodic structure is different from others, which are etched on the same surface of planar waveguide by integrating. This offers a huge advantage for fabrication and compaction. In practical applications, the wavelengths can be relaxed to quasi-monochromatic light due to the symmetry of the in-coupler and out-coupler. Moreover, by adding the sub-grating period to optimization variables while ensuring the common period constant, the final grating could be further optimized to get better results, such as higher diffraction efficiency and less stray light, but the cycle of design will be longer and the structure will be more complex. The fabrication of the microstructure could be etched by E-beam or I-beam, and it could be duplicated. The optical system could be as thin as micrometers to millimeters as we wish because the optical coupling part is only one stack DOE, which can dramatically reduce the weight and size of devices, providing a lightweight and compact solution for the dispersion problem in diffractive waveguide technology. However, due to the sensitivity of micro/nano elements to the angle of incident light, our current design is limited to the paraxial region, and the structures require high processing precision, under 10 nm or less, which is still a challenge for existing equipment.

5. Conclusions

In this paper, we have proposed a design method and optical systems for an achromatic surface microstructure, which is composed with one triple-carved-sub-grating. Under TE polarization, the simulation results proved that the designed surface microstructure can diffract RGB lights achromatically. This surface microstructure could be duplicated and used in NEDs as the coupling optics, providing a lightweight and compact solution for the dispersion problem in diffractive waveguide technology, such as head-mounted display and wearable display in the future. This method and system could be one possibility to eliminate dispersion both horizontally and vertically simultaneously and independently. Because its light weight, compact size, easy duplication, cheap price, portability, and flexibility, it is a promising technology to bring about the Augmented Reality (AR) glasses similar to our normal glasses in our future daily life.

Funding information

National Key R&D Program of China (2017YFB1002900); National Natural Science Founding of China (NSFC) (61575024, 61420106014) and the UK Government's Newton Fund.

References

- [1] J. Rolland, K. Thompson, See-through head worn displays for mobile augmented reality, *Proc. China Natl. Comput. Conf.* 7 (8) (2011) 2837.
- [2] B. Kress, T. Starner, A review of head-mounted displays (HMD) technologies and applications for consumer electronics, *Proc. SPIE* (2013) 87200A–87200A.
- [3] Ricardo Martins, Vesselin Shaoulov, Yonggang Ha, Jannick Rolland, A mobile head-worn projection display, *Opt. Express* 15 (22) (2007) 14530–14538.
- [4] Masayuki Takagi, Toshiaki Miyao, Takahiro Totani, Akira Komatsu, Takashi Takeda, Light guide plate and virtual image display apparatus having the same, US patent, US8662686 (2014).
- [5] Dewen Cheng, Yongtian Wang, Hong Hua, M.M. Talha, Design of an optical see-through head-mounted display with a low f-number and large field of view using a freeform prism, *Appl. Opt.* 48 (14) (2009) 2655–2668.
- [6] Andrew Maimone, Andreas Georgiou, Joel Kollin, Holographic near-eye displays for virtual and augmented reality, *ACM Trans. Graph.* 36 (4) (2017) 1–16.
- [7] P. Saarikko, Diffractive exit-pupil expander for spherical light guide virtual displays designed for near-distance viewing, *J. Opt. A* 11 (6) (2009) 065504.
- [8] Jian Han, Juan Liu, Xincheng Yao, Yongtian Wang, Portable waveguide display system with a large field of view by integrating freeform elements and volume holograms, *Opt. Express* 23 (3) (2015) 3534–3549.
- [9] Dewen Cheng, Yongtian Wang, Chen Xu, Weitao Song, Guofan Jin, Design of an ultra-thin near-eye display with geometrical waveguide and freeform optics, *Opt. Express* 22 (17) (2014) 20705–20719.
- [10] K. Sarayeddine, K. Mirza, Key challenges to affordable see-through wearable displays: the missing link for mobile ar mass deployment, *Proc. SPIE* 8720 (2013) 87200D–87200D.
- [11] F. Aieta, M.A. Kats, P. Genevet, F. Capasso, Multiwavelength achromatic metasurfaces by dispersive phase compensation, *Science* 347 (6228) (2015) 1342–1345.
- [12] K. Mohammadreza, A. Francesco, K. Pritpal, M.A. Kats, G. Patrice, R. David, Federico Capasso, Achromatic metasurface lens at telecommunication wavelengths, *Nano Lett.* 15 (8) (2015) 5358.
- [13] Z.L. Deng, S. Zhang, G.P. Wang, A facile grating approach towards broadband, wide-angle and high-efficiency holographic metasurfaces, *Nanoscale* 8 (3) (2016) 1588–1594.
- [14] H. Mukawa, K. Akutsu, I. Matsumura, S. Nakano, T. Yoshida, M. Kuwahara, K. Aiki, M. Ogawa, 8.4: distinguished paper: a full color eyewear display using holographic planar waveguides, *SID Symposium Digest of Technical Papers* 39(1) (2008) 89–92.
- [15] Rui Shi, Juan Liu, Haozhi Zhao, Zhengming Wu, Yu Liu, Yu Hu, Yunming Chen, Jinghui Xie, Yongtian Wang, Chromatic dispersion correction in planar waveguide using one-layer volume holograms based on three-step exposure, *Appl. Opt.* 51 (20) (2012) 4703–4708.
- [16] Nannan Zhang, Juan Liu, Jian Han, Xin Li, Fei Yang, Xugang Wang, Bin Hu, Yongtian Wang, Improved holographic waveguide display system, *Appl. Opt.* 54 (12) (2015) 3645–3649.
- [17] Simmonds, Michael David, M.S. Valera, Display comprising an optical waveguide and switchable diffraction gratings and method of producing the same, US patent, US9664824B2 (2017).
- [18] Gregory P. Crawford, Electrically switchable bragg gratings, *Opt. Photonics News* 14 (4) (2003) 54–59.
- [19] <https://www.microsoft.com/microsoft-hololens/en-us>.
- [20] M.G. Moharam, Eric B. Grann, Drew A. Pomett, T.K. Gaylord, Formulation for stable and efficient implementation of the rigorous coupled-wave analysis of binary gratings, *J. Opt. Soc. Amer. A* 12 (5) (1995) 1068–1076.
- [21] <https://www.image-engineering.de/>.